Characteristics of the nanostructures in thermal sprayed hydroxyapatite coatings and their influence on coating properties

Li, H.; Khor, Khiam Aik

2006

Li, H., & Khor, K. A. (2006). Characteristics of the nanostructures in thermal sprayed hydroxyapatite coatings and their influence on coating properties. Surface and Coatings Technology, 201(6), 2147-2154.

https://hdl.handle.net/10356/95500

https://doi.org/10.1016/j.surfcoat.2006.03.024

Characteristics of the nanostructures in thermal sprayed hydroxyapatite coatings and their influence on coating properties

H. Li*, K.A. Khor
School of Mechanical and Aerospace Engineering
Nanyang Technological University, Singapore

Abstract

There are generally two methods for depositing nanostructured coatings, retaining nanostructures from starting feedstock and forming novel nanostructures through quenching. The present study utilized spray-dried nanostructured hydroxyapatite (nSD-HA) feedstock for coating/splat deposition. The nanostructures were characterized by transmission electron microscopy (TEM) and field emission scanning electron microscopy (FESEM). Results revealed that the rod-shaped nano- grains in the starting HA particles (<500nm in length and 40-70nm in diameter) encountered two major experiences: enlargement due to unmelt state and reorganization due to melting-solidification. The molten part of the particles results in formation of spherical nanosized particles with grain sizes of 30-110nm. TEM observation of the HA splats demonstrates consistent nanostructures. The unmelted part of individual nSD-HA particles showed significantly enlarged grains along radial direction (<550nm in length and <400nm in diameter). In addition, individual hexagonal grains were observed in the HVOF coating made from 30±10μm powder. The grains have the size of <250nm in height and <50nm in side length and are perpendicular to the coating/substrate interface. The nanostructures within the coatings contribute to an increased Young's modulus with up to 60.11GPa, however, they showed detrimental effect on adhesion of the coatings. *In vitro* cell culturing revealed marked attachment and proliferation of the osteoblast cells on the nanostructured coatings. However, the results suggest that the nanostructures possess less importance than the phases (preferably high crystalline HA) on enhancing the cell proliferation.

Key words: Hydroxyapatite coating; Nanostructures; Splats; Adhesive strength; Young's modulus; Cell culture.

1. Introduction

Nanostructured coatings attracted intense attentions in recent years due to their enhanced mechanical properties [1-5]. Basically, there are two approaches for fabricating nanostructures in thermal sprayed coatings, retaining nanostructures from starting nanophase/nanostructured feedstock [5-7] and spray-forming nanostructures owing to the rapid cooling of the droplets upon their impingement [3,8]. To date, however, the knowledge about the nanostructured coatings is still insufficient. It is believed that the use of nanostructured feedstock might be a promising way for deposition of nanostructured coatings. Generally, the spray powder can be fabricated through agglomerating nanosized particles to form big ones [3,5]. Calcium phosphate (CP) coatings deposited on titanium alloys have

* Corresponding author. Tel: +65 – 6790 4351, fax: +65 – 6792 4062. Email: mhli@ntu.edu.sg (H. Li).

shown promising effects on rapid bone remodeling and suitable functional life in orthopedic and dental applications. Extensive studies revealed that the long-term performance and functional service duration of the hydroxyapatite (HA)-coated implants are influenced significantly by the microstructure of the coatings [9,10]. In addition, recent *in vitro* study has reported that nano-sized ceramics (Al_2O_3, TiO_2) possess significant ability to decrease apoptotic cell death and hence improve cell proliferation [11]. Previous *in vitro* study also showed that nano-sized ceramics enhanced osteoblast adhesion on them [12]. However, it is unclear yet if nano-sized grains within a biocompatible coating could promote cell proliferation. In the present study, spray-dried HA powder with nanostructures (nSD-HA) was sprayed using both plasma and HVOF spray processes. The nanostructures in the HA coatings were characterized and their influence on coating properties was studied. Furthermore, individual HA splats were characterized for a purpose of further elucidating the nanostructures in the coatings. The influence of the nanostructures on *in vitro* proliferation of the osteoblast cells was also investigated.

2. Materials and testing methods

The nSD-HA powder synthesized in-house via the wet chemical method was utilized for the coating deposition on Ti-6Al-4V substrates employing both HVOF and plasma spray techniques. The powder was heat-treated at 950ºC for 1.5h and XRD detections were performed to ensure their major component as stoichiometric HA. Close examination of the spherical individual particles shows the nanostructures with rod-shaped grains <500nm in length and 40-70nm in diameter (Fig. 1). A nanostructured HA particle is formed by the agglomeration of the individual rod-shaped nanosized HA grains. A fully computerized HV2000 HVOF system (*PRAXAIR*, USA) with a nozzle diameter of 19 mm and SG100 plasma system (*PRAXAIR*, USA) were utilized for the spraying. The spray parameters are tabulated in Table 1. For the HVOF spraying, the HA powder with different particle size ranges, 50±10μm, 40±10μm, 30±10μm, was used with an aim to clarify the influence of melt state of the powder on the nanostructural features. The size distribution of the powder was determined by a laser particle size analyzer (analysette 22 NanoTec, FRITSCH, Germany).

Microstructure of the samples was observed using scanning electron microscopy (SEM, JEOL JSM-5600LV), field emission SEM (FESEM, JEOL JSM-6340F), and transmission electron microscopy (TEM, JEOL, JEM-2010) operated at 200 kV. In order to get ready-for-observation splat samples for TEM surface characterization, the HA droplets were directly sprayed onto copper discs (3.05 mm in diameter, 200 square mesh), which can be directly utilized for TEM observation. The copper discs were attached intimately on polished Ti-6Al-4V plate. Phase composition of the starting powder and as-sprayed coatings was analyzed by means of XRD (MPD 1880, Philips, The Netherlands). The operating conditions were 40 kV and 30 mA by using Cu K_α radiation. The goniometer was set at a scan rate of 0.02°/s over a 2θ range of 20-60°. The adhesive bonding strength of the HA coatings was determined according to the ASTM C633-79 standard. A universal testing system, Instron 4204, was used for the adhesive strength measurement with a tensile speed of 1mm/min. 5 samples were tested for an average value. Young's modulus of the coatings was measured through a microindentation test approach (CSEM® MHT, Switzerland). The detailed information has been described in other paper [13]. The indentation was applied on polished cross-sections of the coatings. The maximum load was 1 N with the loading rate of 1 N/min and the pause was 10 s. The unloading rate was 1 N/min. The Poisson's ratio of the coatings was assumed to be 0.28 [14], and the elastic properties of the diamond indenter used in the calculations were E_i = 1141 GPa and ν_i = 0.07 according to the CSEM Microhardness Tester Manual. In total, 15 points were conducted on polished cross-sections of the coatings.

The *in vitro* cell culture work was conducted for the coatings and nSD-HA powder using the hFOB 1.19 cell line. This line was established by transfection of limb tissue obtained from a spontaneous miscarriage. The coating samples, which have the dimension of 10mm×10mm in width and length respectively, were incubated in 24-well plate. The nanostructured HA coatings had a thickness of ~100μm on 2mm thick Ti6Al4V substrates. In the present study, *in vitro* osteoblast behavior of the nSD-HA powder with different particle size ranges, <20μm, -45+20μm, -75+45μm, and -100+75μm, were also studied through being incubated in Dulbecco's modified eagle medium (DMEM) containing 10% fetal bovine serum (FBS) and 0.5% antibiotics. Before the incubation, the coating samples were autoclaved and the powder particles were sterilized by ultraviolet irradiation for 24 h. The sterilized powder with 10mg and the coating samples were incubated in 1ml medium with 5×10^4 cells. Cells were cultured in an atmosphere of 100% humidity and 5% CO_2 at 37°C in 24-well culture plates (with 1ml media contained in each well). Media were changed at 48 hrs intervals. The powder was incubated for 2 days, 4 days, and 6 days for comparison purpose. The methyl thiazole tetrazodium (MTT) assay was employed to examine the proliferation of the cells. The plates were read using 490nm wavelength on a microplate reader machine (Benchmark Plus, Bio-Rad Laboratories Inc.). Every plate was read for 3 times and each type of the coatings/powder had 3 samples. The morphology of the cells attached onto the suspended particles was observed by optical microscope. SEM observation of the cells attached/proliferated on the coating surface was also conducted. Prior to the SEM observation, 2.5% glutaraldehyde in 0.1M sodium cacodylate buffer was used for pre-fixing the cells, followed by post fixation with 1% osmium tetroxidein in 0.1M cacodylate buffer. The final steps for fixing the samples were dehydration and critical point drying.

3. Results and discussion

Previous study has shown that the starting powder size played a key role in determining the microstructures of the HVOF coatings [15], the effect was attributed to the alternative melt state of the particles. The present study therefore investigated the HVOF coatings made from the powder with different particle size ranges. The HA coatings show clearly the evidence of the presence of nanostructures at both their surface and cross-sections (Fig. 2). The grain sizes of the starting powder and coatings are summarized in Table 2. Similar grain sizes can be seen at both the coating surface and cross-sections. In addition, the plasma sprayed HA coatings also show predominate presence of the nanostructures. However, the sizes of the grains (40-90nm) are slightly smaller than those of the grains in the HVOF coatings (50-110nm). FESEM observation from the bottom side of the coating (the area with intimate contact with the substrate) shows interesting microstructures (Fig. 3). That is, the HVOF sprayed coatings made from the smallest powder (30±10μm) exhibit typical individual grains with hexagonal prismatic morphology (Fig. 3a). Most of the grains exhibit a size of <250nm in height and <50nm in side length (Fig. 3a-1). Very rare of them have the enlarged size of 0.4-1.2μm in height and 80-120nm in width. Whilst other coatings do not have such features (Fig. 3b,c). Previous investigation on sprayed particles has given evidence of different melt state of the powder during the HVOF spraying [16]. It is further confirmed in this study that during the HVOF spraying, bigger powder particles experienced partial melt state, while the smallest particles were subjected to a full melt state. Plasma sprayed HA particles achieved a full melt state. There is no doubt that the melting of the particles accounts for the reorganization of the rod-shaped nanosized grains in the starting feedstock. The formation of the nanosized grains with hexagonal prismatic morphology indicates the influence of both the melt-state and temperature of the HA particles upon their impingement. The partial melt state during HVOF spraying and overheating state during plasma spraying of the HA particles could result in a

faster cooling rate of the molten part upon their impingement on the room-temperature substrate. The high cooling rate would influence the formation of the hexagonal grains. Although Chraska et al. reported their findings that the top surface of the first solidified splat causes epitaxial growth of columnar grains in subsequent splats for plasma sprayed YSZ splats [17], the present study revealed spherical nanosized grains within the second folded splat and there is no experimental evidence showing presence of columnar grains in other parts in the coatings other than in the first layer splats.

It is noted that the nanostructures in all the coatings showed markedly different features from those in the starting feedstock (Fig. 1b). After the high temperature spray processing, the rod-shaped nano- grains have turned to be nanosized spheres (with the size of 30nm ~ 120nm, Table 2). This suggests that during the melting/resolidification process, individual nano-rods were mostly fractured into several individual parts, and with the aid of surface tension, the nanosized spheres were accomplished. Therefore, it can be expected that finer nanostructures in starting feedstock would induce finer nanostructures in the coatings. It nevertheless indicates that the existence of nanosized grains in the starting feedstock is essential for formation of nanostructures in the coatings.

TEM and FESEM observation of the HA splats further reveals the presence of the nanostructures (Fig. 4). It is clear that at the areas near to splats' fringes, the structure is actually nanostructures composed of ~30nm grains (Fig. 4a,b). As mentioned earlier, the HA particles actually encounter different melt states during HVOF and plasma spraying. This may influence both the microstructure and phases in the resultant splats/coatings. The unmelted part of the HVOF sprayed HA splat was also characterized using TEM. The sample was prepared through further ion milling the individual HA splats. As shown in Fig. 4c, the unmelted part of the splat shows enlarged rod-shaped grains with the dimension of <400nm in diameter and <550nm in length. The HVOF coating made from partially melted powder, hence, must have a mixed nano- and micro-structure. Enhanced cooling of substrate during coating deposition could effectively increase the content of the nanosized grains in the HA coatings. The nanostructures exhibited within the molten part of the HA splats are consistent with the nanosized grains revealed in the coatings. This on the other hand further suggests that during the accumulation of individual HA splats to form bulk coating, there is no obvious grain growth for the nanosized grains. The possible changes experienced by the nanostructured feedstock are schematically depicted in Fig. 5.

Influence of the nanostructures on the mechanical properties in terms of adhesive strength and Young's modulus was evaluated (Fig. 6). It is found that the nanostructures contribute to increased Young's modulus values. With the increase of the melted area in the spayed particles (hence the relative content of the nanostructures, HVOF3 vs. HVOF1 in Fig. 6a), the Young's modulus of the corresponding coatings increases. However, they showed detrimental effect on adhesive strength (Fig. 6b). Tensile failure analysis has suggested an entire adhesive failure mode. This in turn indicates that the coating/substrate interface plays a key role in determining the adhesion. The comparison among the HVOF coatings suggests a weak bonding of the big hexagonal grains with the substrate (Figs. 3, 6). The perpendicular-to-substrate grains might have changed the residual stresses at the coating/substrate interface, or they weakened the mechanical interlocking of the coating with the rough substrate. For a high adhesive strength, formation of the grains with hexagonal prismatic morphology near to the coating/substrate interface must be avoided. The mechanism why the nanostructures benefit high Young's modulus is not clear yet. The presence of nanosized pores among the nanosized grains might be responsible for the increased value, as it has been discussed that irregular pores and large pores can result in decreased modulus [18,19]. Furthermore, high packing density of constituent atom exhibit high values of elastic modulus [20]. Although the plasma sprayed HA coating comprises compatible content of nanostructures, both the low Young's

modulus and adhesive strength might be related to the phases present in the coating and the low velocity of in-flight particles (this brought about high porosity). It has been clarified in the present study that the plasma sprayed HA coating exhibited a lower crystallinity and more severe HA decomposition than HVOF coatings (Fig. 7a). For a comparison purpose, the XRD pattern of the starting HA powder was also shown (Fig. 7b), which shows the evidence of full crystalline HA structure. It must be noted that within the nanostructures in the splats, there are many phases apart from HA, e.g., ACP, α-TCP, β-TCP, being revealed. These may not be desirable since these phases come from HA decomposition and have less bioactivity than HA [21,22]. Furthermore, the presence of the phases in the plasma-sprayed HA coating may also account for the low modulus of the coating.

There has been no doubt that HA and HA-based composites are capable of enhancing attachment and proliferation of viable cells [23-28]. The present study further showed clear evidence of significantly different cell proliferation rates on the surface of the nanostructured HA coatings ($t<0.05$, paired students' *t*-distribution). The attachment of the cells on the coating surface is typically shown in Fig. 8a. Coatings with more crystalline HA (Fig. 7) exhibit higher cell proliferation rate (Fig. 8b). Apparently, the plasma sprayed coating with fine nanosized grains possesses more surface areas than the HVOF coatings. However, the plasma sprayed HA coating exhibits the lowest cell proliferation rate. It must be noted that the plasma sprayed coating showed obvious presence of TCP, ACP, etc, which resulted from the HA decomposition due to the high temperature of the plasma jet. These phases have remarkably different bioactivity from crystalline HA, e.g., higher dissolution rate into medium etc [21,22,29] and therefore influence the cell behaviors during the culturing. Since increased surface area undoubtedly furthers cell proliferation, it can be claimed that the nanostructures play less important role than the phases on the attachment/proliferation of the cells. Although some researchers found that dissolution of the Ca-rich phases was accompanied by good cell attachment [30] and high proliferation rate [31]. The influence of the phases at the coating surface is yet far from reaching a final verdict. In order to further reveal the influence of the surface area on the cell behavior, the nSD-HA powder with different particle size ranges was studied. The cells attached onto the nSD-HA particles very well (Fig. 9a). Results show that all the powder brought about significant cell proliferation compared to control (revealed through the MTT assay). Fast proliferation was achieved within 2 days (Fig. 9b). It is obvious that with the same weight (10mg), the powder with smaller particle sizes means more particles, and hence more particle boundary area. The boundary area of the powder with different particle size ranges is in inverse proportion to the diameter of the particles. The increased particle boundary surface area, which was exposed to the osteoblast cells, must be responsible for the promoted cell proliferation. However, even though it is noted that the smaller nSD-HA powder particles demonstrate enhanced cell proliferation compared to bigger particles, the differences among the powder are not significant. Even though it was reported that there was increased adhesion with nanophase materials due to the increased surface boundaries [32], the present study indicates that the bioactivity of the coatings is more dependent on phases than on the nanostructures. Meanwhile, how the nanostructures in HA coatings take effect on the cell proliferation is not clear yet. Nevertheless, the HA coatings with high content of both crystalline HA and nanostructures are favorably preferred for their biomedical applications.

4. Conclusions

Nanostructured HA coatings with the grain sizes of as small as 30nm have been produced using nSD-HA feedstock. Refining of the rod-shaped nanosized grains in the starting particles was achieved due to the melting/rapid-solidification. Overheating of the nSD-HA particles

during plasma spraying resulted in formation of fine grains (30-90nm), whilst partially unmelted part of the particles during HVOF spraying accounted for enlarged grains (<400nm in diameter and <550 in length). The coatings with more nanostructures exhibited higher Young's modulus of up to 60.11GPa. However, a detrimental effect of the nanostructures on adhesion was revealed which is possibly due to the presence of the enlarged grains with hexagonal prismatic morphology perpendicular to the substrate at the coating/substrate interface. *In vitro* cell culturing experiment further suggests a more important role of phases (preferably crystalline HA) than the nanostructures/boundary-areas within the coatings on promoting proliferation of the osteoblast cells.

Acknowledgements

The author, H. Li, acknowledges the Singapore Millennium Foundation (SMF) for its post-doctoral research fellowship. The authors also thank Dr. Y. Gu for her help in observing the nanostructures using FESEM.

References

[1]. Y.C. Zhu, K. Yukimura, C.X. Ding, P.Y. Zhang, Thin Solid Films 388 (2001) 277.

[2]. C.C. Berndt, editor, Thermal spray processing of nanoscale materials II – extended abstracts, J. Therm. Spray Technol. 10 (2001) 147.

[3]. S.C. Tjong, H. Chen, Mater. Sci. Eng. R: Reports 45 (2004) 1.

[4]. J.F. Li, H. Liao, X.Y. Wang, C. Coddet, H. Chen, C.X. Ding, Thin Solid Films 460 (2004) 101.

[5]. M. Gell, E.H. Jordan, Y.H. Sohn, D. Goberman, L. Shaw, T.D. Xiao, Surf. Coat. Technol. 146 (2001) 48.

[6]. P. Bansal, N.P. Padture, A. Vasiliev, Acta Materi. 51 (2003) 2959.

[7]. R.S. Lima, A. Kucuk, C.C. Berndt, Mater. Sci. Eng. A 313 (2001) 75.

[8]. J. Gang, J.P. Morniroli, T. Grosdidier, Scrip. Mater. 48 (2003) 1599.

[9]. E. Suominen, A.J. Aho, E. Vedel, I. Kangasniemi, E. Uusipaikka, A. Yli-Urpo, J. Biomed. Mater. Res. 32 (1996) 543.

[10]. J.A. Szivek, P.L. Anderson, T.J. Dishongh, D.W. de Young, J. Biomed. Mater. Res. 33 (1996) 121.

[11]. L.G. Gutwein, T.J. Webster, Biomaterials 25 (2004) 4175.

[12]. T.J. Webster, R.W. Siegel, R. Bizios, Biomaterials 20 (1999) 1221.

[13]. H. Li, K.A. Khor, P. Cheang, Surf. Coat. Technol. 155 (2002) 21.

[14]. H. Aoki, Medical Applications of Hydroxyapatite, Ishiyaku EuroAmerica, Inc., Tokyo, st.Louis, 1994.

[15]. H. Li, K.A. Khor, P. Cheang, Mater. Sci. Eng. A 293 (2000) 71.

[16]. K.A. Khor, H. Li, P. Cheang, Biomaterials 25 (2004) 1177.

[17]. T. Chraska, A.H. King, Thin Solid Films 397 (2001) 40.

[18]. I. Sevostianov, M. Kachanov, Acta Mater. 48 (2000) 1361.

[19]. T.D. Shen, C.C. Koch, T.Y. Tsui, G.M. Pharr, J. Mater. Res. 10 (1995) 2892.

[20]. N. Soga, J. Non-Cryst. Solids 52 (1982) 365.

[21]. P. Ducheyne, S. Radin, L. King, J. Biomed. Mater. Res. 27 (1993) 25.

[22]. L. Cleries, J.M. Fernandez-Pradas, J.L. Morenza, Biomaterials 21 (2000) 1861.

[23]. D.D. Deligianni, N.D. Katsala, P.G. Koutsoukos, Y.F. Missirlis, Biomaterials 22 (2001) 87.

[24]. F.R. Rose, L.A. Cyster, D.M. Grant, C.A. Scotchford, S.M. Howdle, K.M. Kevin, M. Shakesheff, Biomaterials 25 (2004) 5507.

[25]. L.E. Carey, H.H.K. Xu, C.G. Simon, S. Takagi, L.C. Chow, Biomaterials 26 (2005) 5002.

[26]. M. Hossain, R. Irwin, M.J. Baumann, L.R. McCabe, Biomaterials 26 (2005) 2595.

[27]. C. Knabe, C.R. Howlett, F. Klar, H. Zreiqat, J. Biomed. Mater. Res. A 71 (2004) 98.

[28]. J.W. Xie, M.J. Baumann, L.R. McCabe, J. Biomed. Mater. Res. A 71 (2004) 108.

[29]. S.H. Maxian, J.P. Zawadsky, M.G. Dunn, J. Biomed. Mater. Res. 27 (1993) 111.

[30]. J. Wang, P. Layrolle, M. Stigter, K. de Groot, Biomaterials 25 (2004) 583.

[31]. H. Kim, G. Georgiou, J.C. Knowles, Y. Koh, H. Kim, Biomaterials 25 (2004) 4203.

[32]. T.J. Webster, J.U. Ejiofor, Biomaterials 25 (2004) 4731.

List of Tables

List of Figures

Plasma spray	HVOF
Net energy: 12 kW Ar: 30.6 l/min He: 22.6 l/min Carrier gas (Ar): 10 l/min Powder feed rate: 10 g/min Spray distance: 120 mm Powder size: 50±10μm	O_2: 283 l/min H_2: 566 l/min Carrier gas (Ar): 19 l/min Powder feed rate: 8 g/min Spray distance: 250 mm Powder size: 50±10μm, 40±10μm, 30±10μm

Table 1

Sample	**Size and features of the nanosized grains (shape)**		
Starting HA powders	40-70nm in diameter, <500nm in length (cylindrical)		
	Coating surface	Inside coating	Near to coating/substrate interface
HVOF coating (50±10μm)	50-100nm (spherical): melted part	50-100nm (spherical): melted part	60-120nm (spherical): melted part
HVOF coating (40±10μm)	50-100nm (spherical)	60-110nm (spherical)	60-120nm (spherical)
HVOF coating (30±10μm)	50-100nm (spherical)	50-100nm (spherical)	Mostly: <250nm in length, <50nm in diameter; Rarely: 80-120nm in width, 0.4-1.2μm in length (rectangular)
Plasma coating (50±10μm)	40-90nm (spherical)	40-90nm (spherical)	30-80nm (spherical)

Table 2

(a)

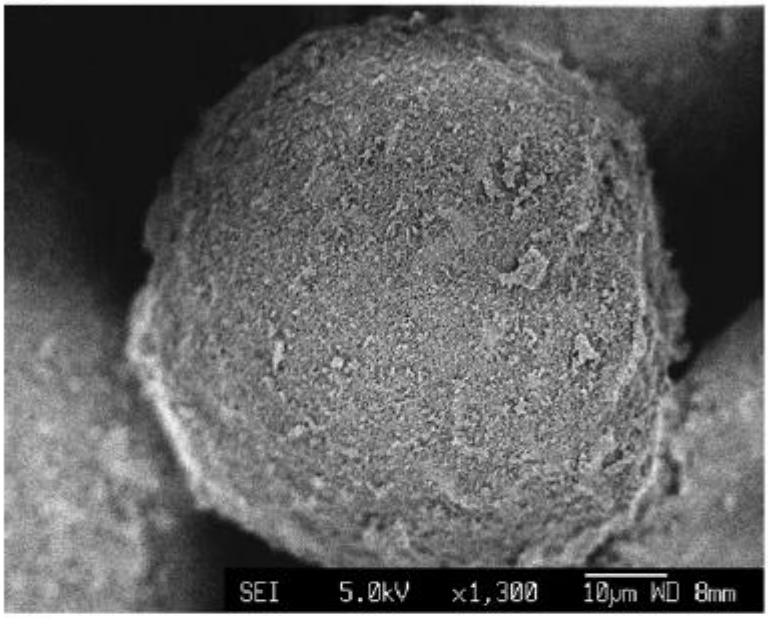

(b)

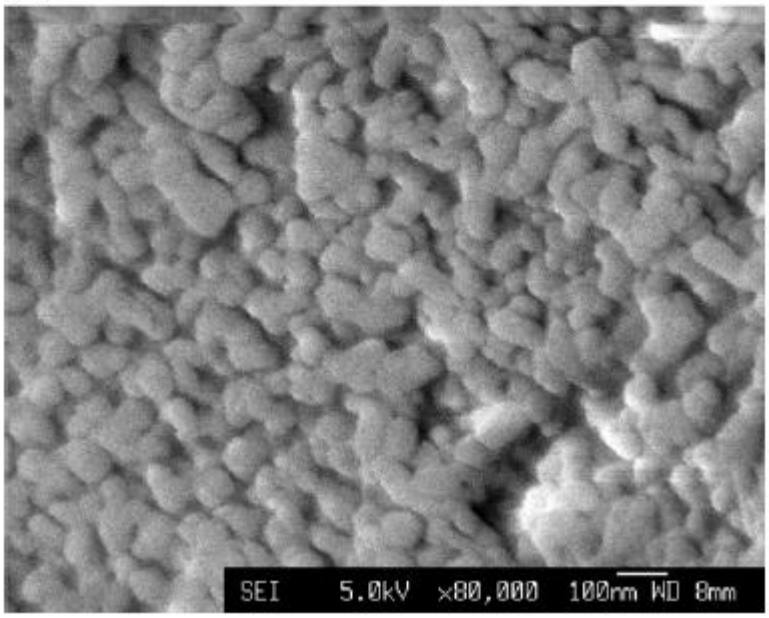

Fig.1

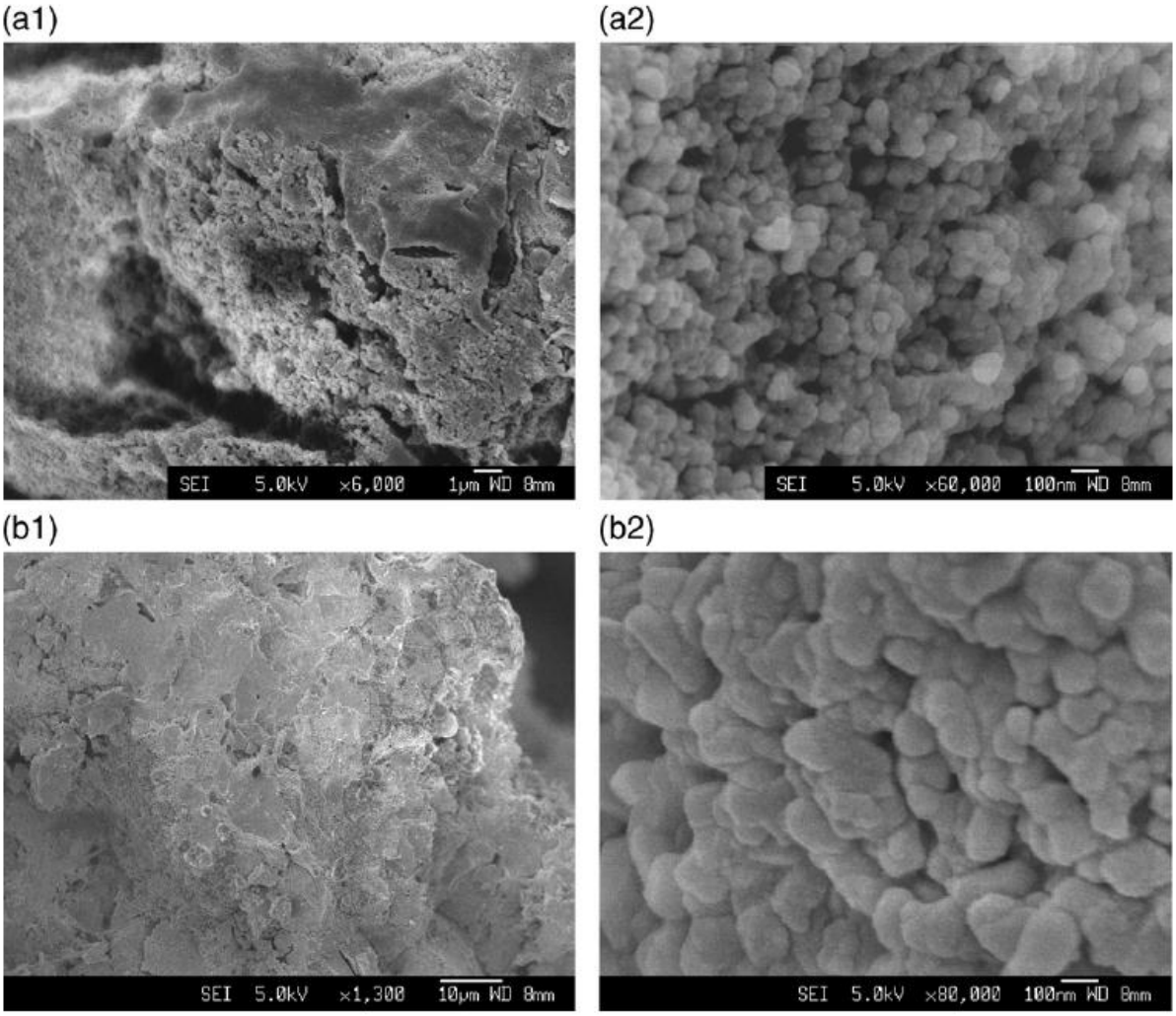
(a1)
SEI 5.0kV ×6,000 1μm WD 8mm
(a2)
SEI 5.0kV ×60,000 100nm WD 8mm
(b1)
SEI 5.0kV ×1,300 10μm WD 8mm
(b2)
SEI 5.0kV ×80,000 100nm WD 8mm

Fig.2

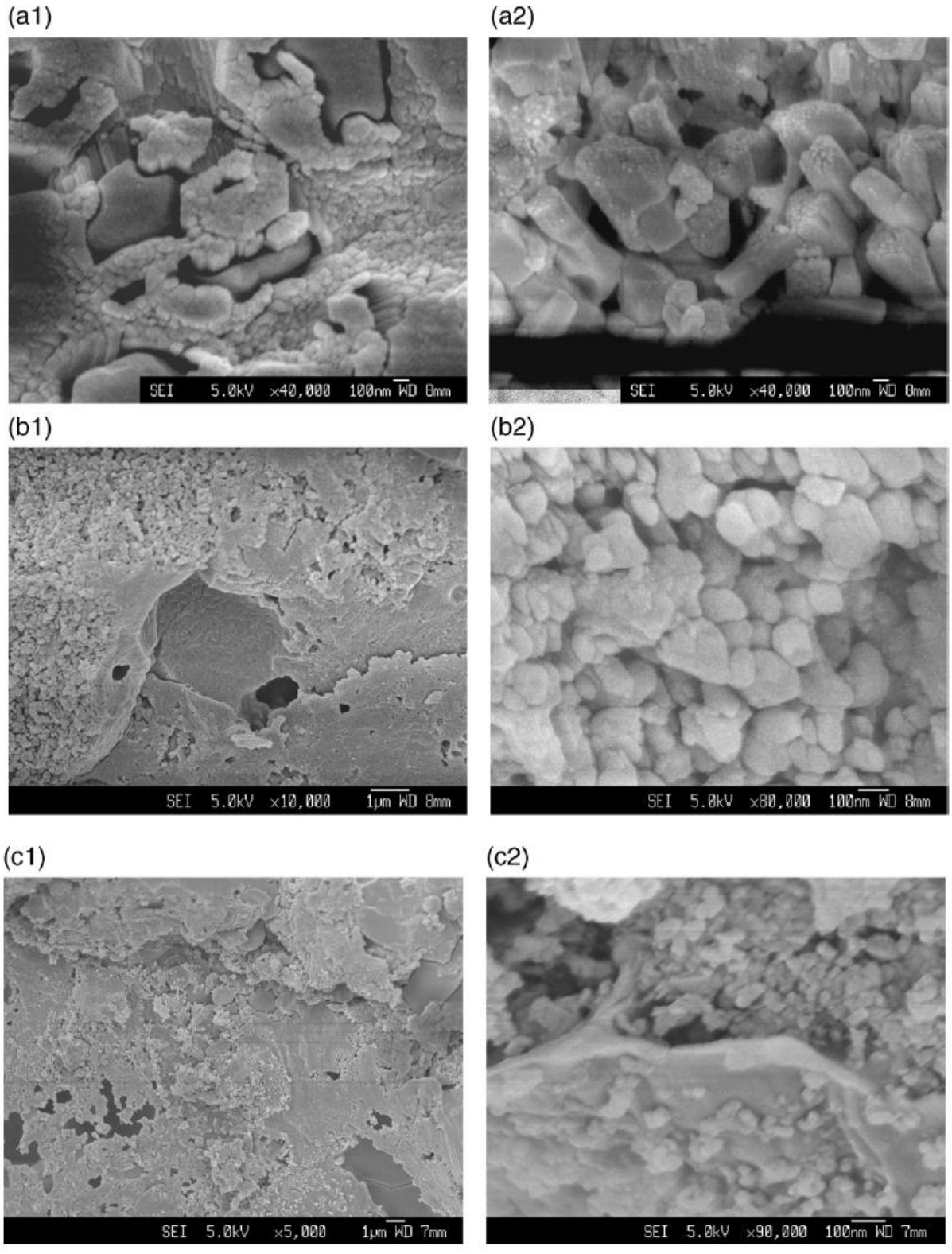
(a1)
SEI 5.0kV x40,000 100nm WD 8mm
(a2)
SEI 5.0kV x40,000 100nm WD 8mm
(b1)
SEI 5.0kV x10,000 1μm WD 8mm
(b2)
SEI 5.0kV x80,000 100nm WD 8mm
(c1)
SEI 5.0kV x5,000 1μm WD 7mm
(c2)
SEI 5.0kV x90,000 100nm WD 7mm

Fig.3

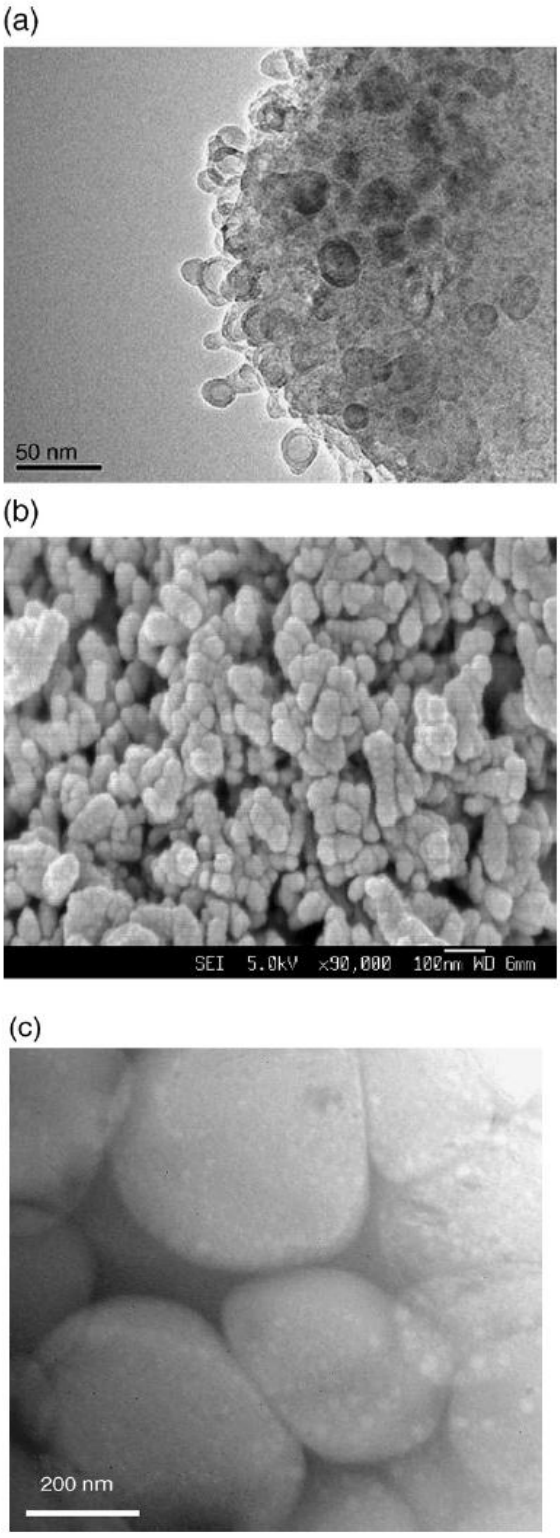

Fig.4

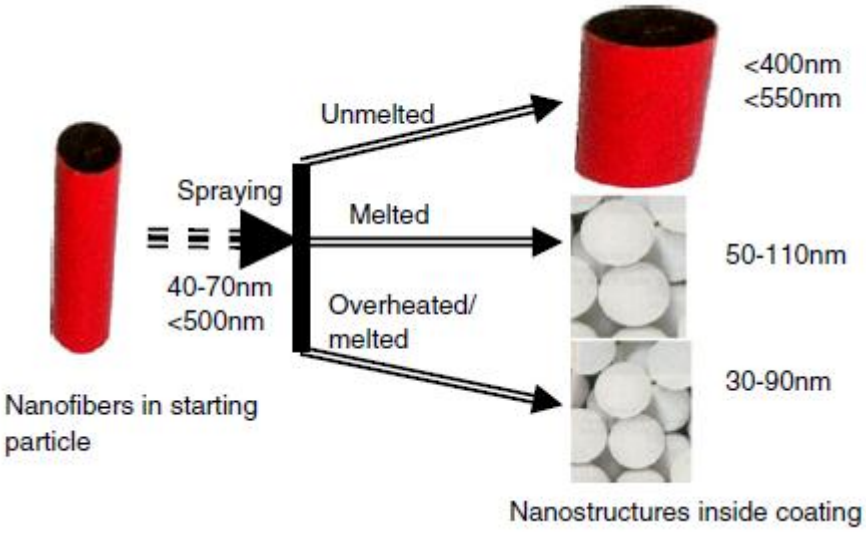
Unmelted
Spraying
Melted
40-70nm
<500nm
Overheated/
melted
<400nm
<550nm
50-110nm
30-90nm
Nanofibers in starting
particle
Nanostructures inside coating

Fig.5

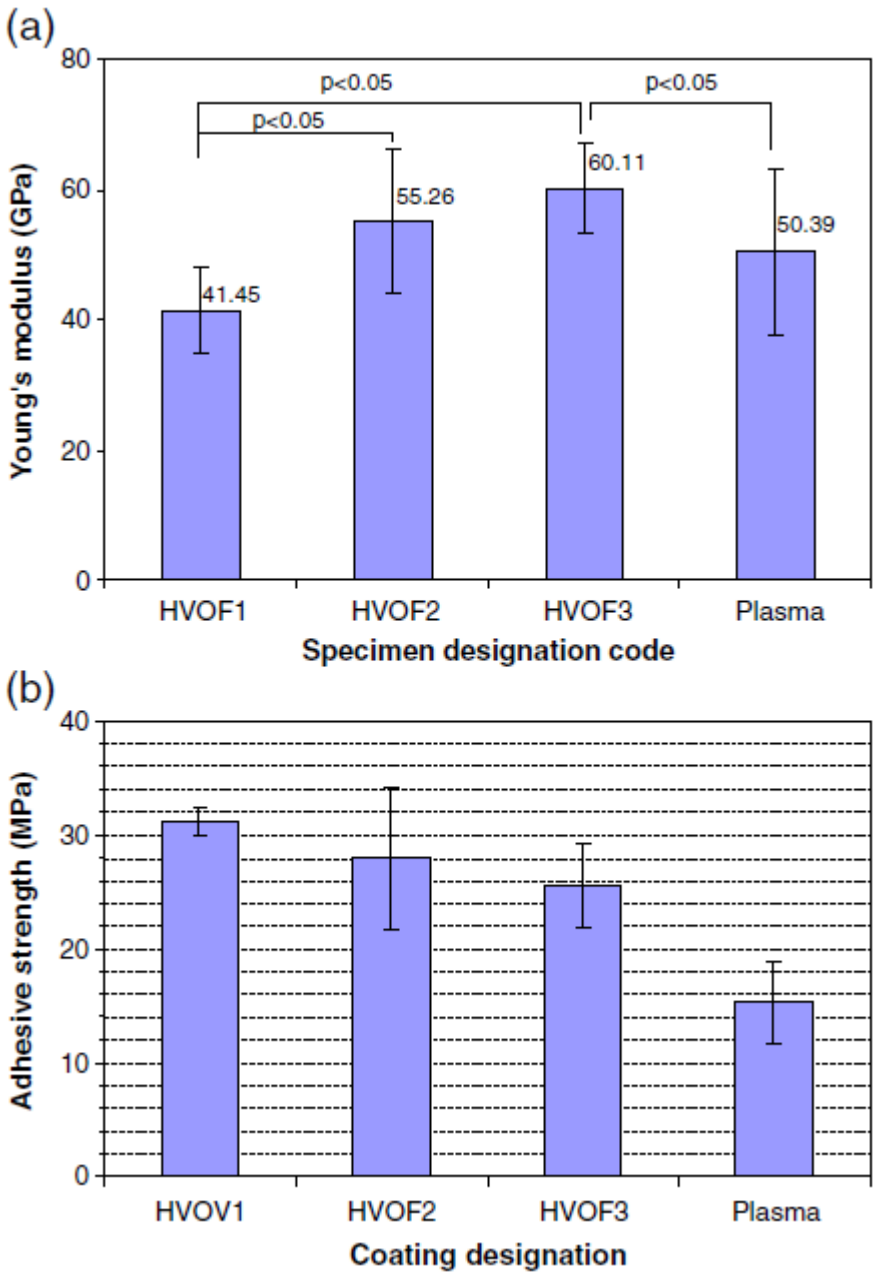
(a)
Young's modulus (GPa)
80
60
40
20
0
p<0.05
p<0.05
p<0.05
41.45
55.26
60.11
50.39
HVOF1
HVOF2
HVOF3
Plasma
Specimen designation code
(b)
Adhesive strength (MPa)
40
30
20
10
0
HVOV1
HVOF2
HVOF3
Plasma
Coating designation

Fig.6

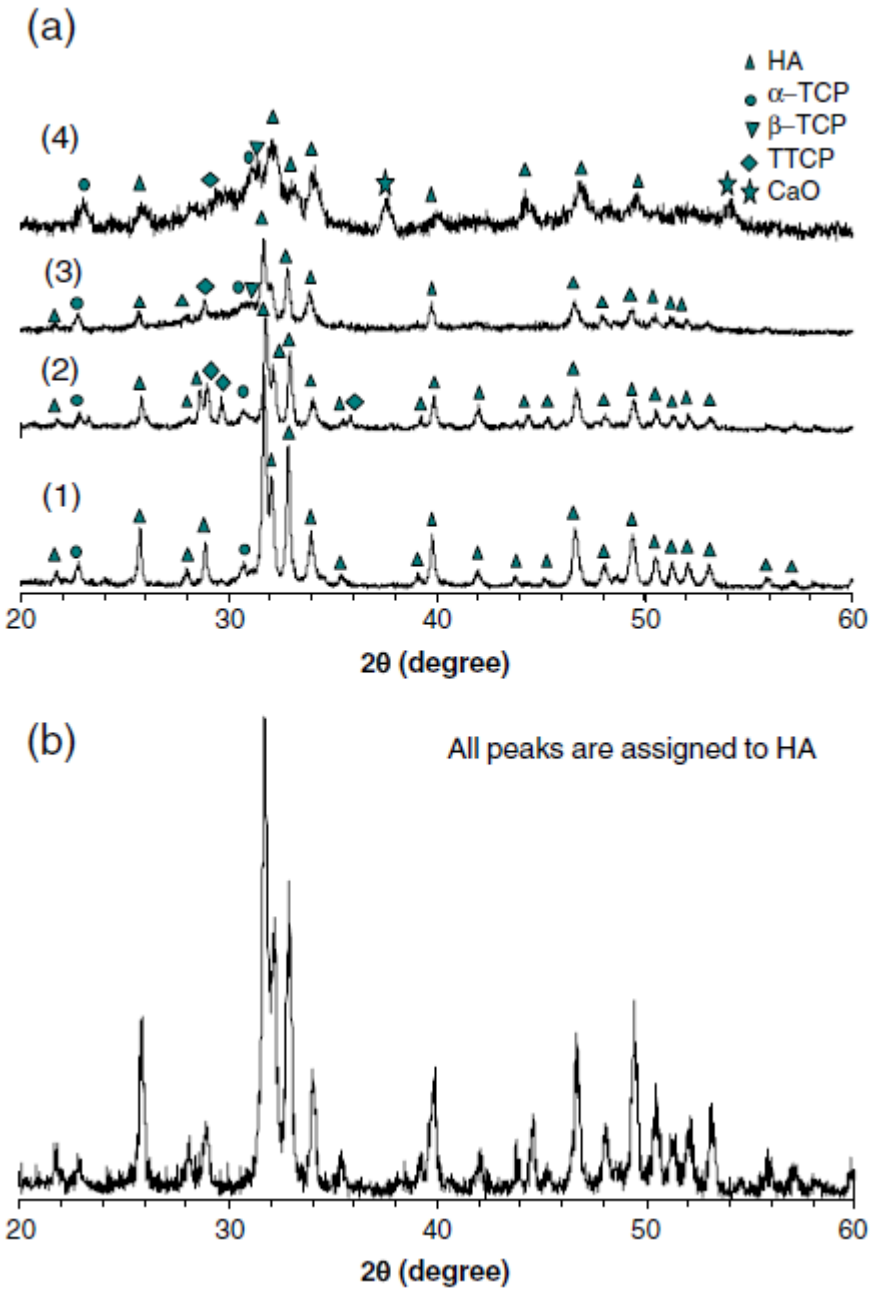
(a)
HA
α–TCP
β–TCP
TTCP
CaO
(4)
(3)
(2)
(1)
20
30
40
50
60
2θ (degree)
(b)
All peaks are assigned to HA
20
30
40
50
60
2θ (degree)

Fig.7

(a)

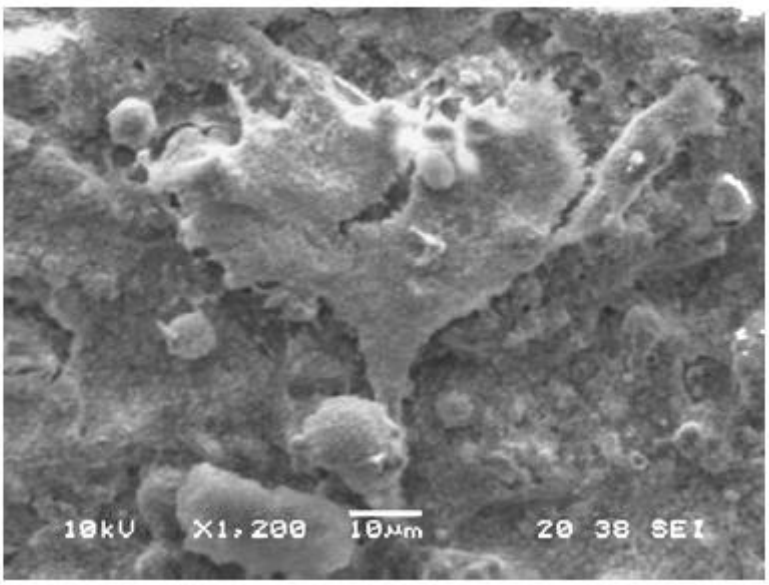
10kV X1,200 10µm 20 38 SEI

(b)

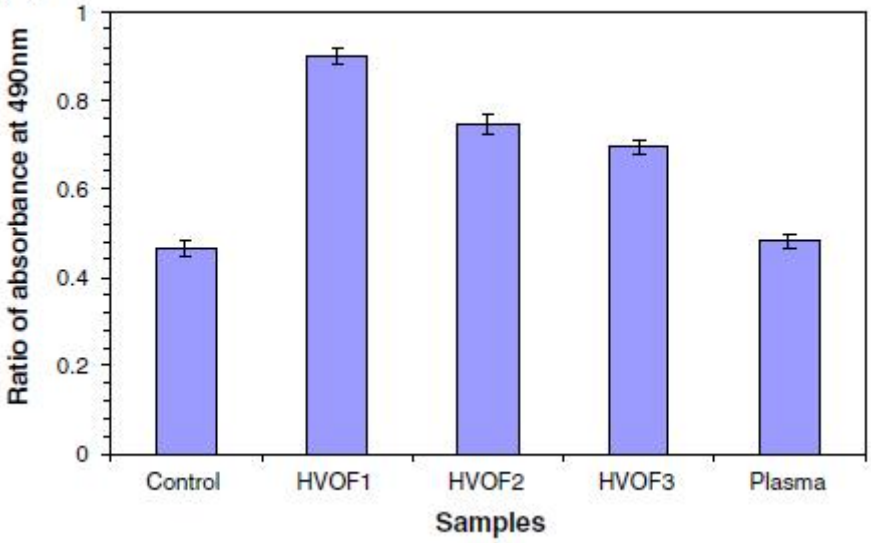
Ratio of absorbance at 490nm
1
0.8
0.6
0.4
0.2
0
Control
HVOF1
HVOF2
HVOF3
Plasma
Samples

Fig.8

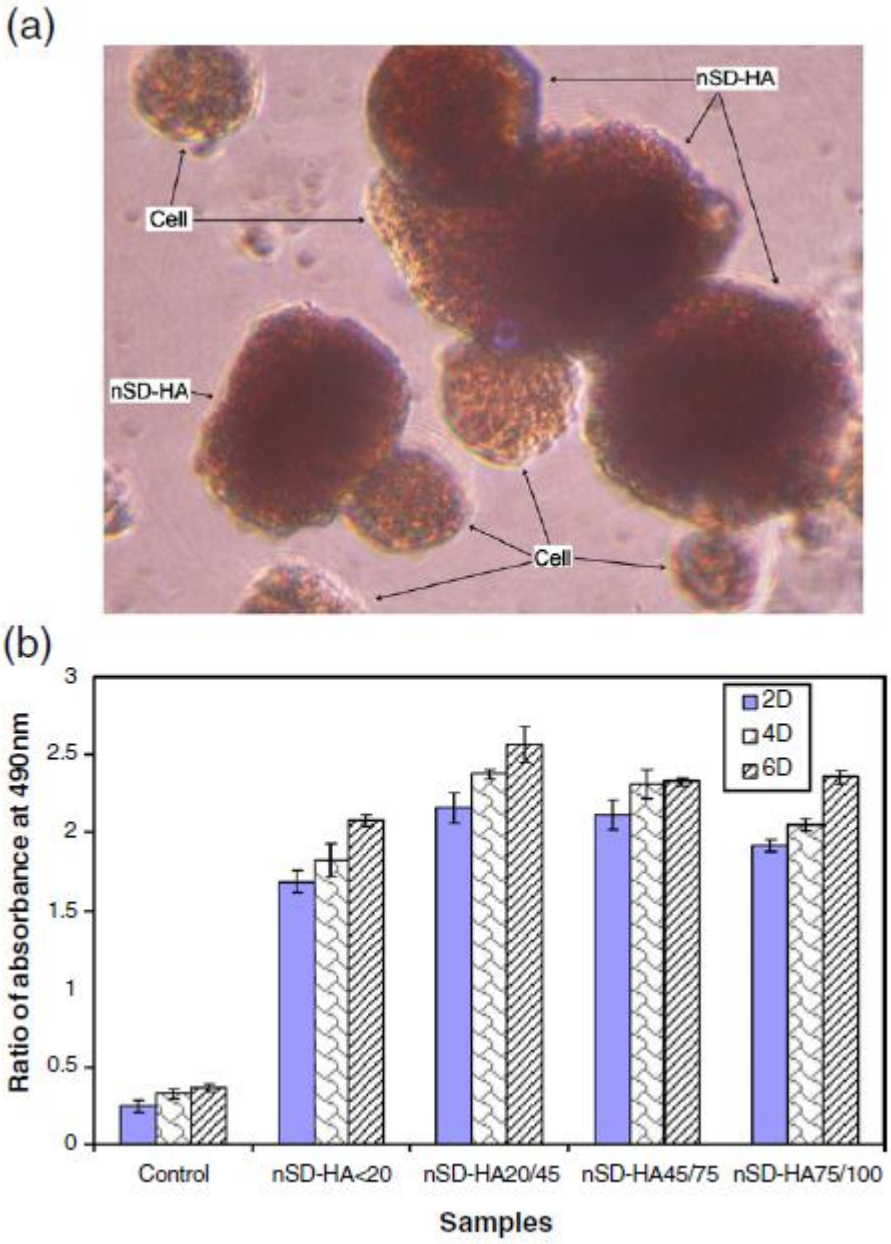
(a)
nSD-HA
Cell
nSD-HA
Cell
(b)
Ratio of absorbance at 490nm
3
2.5
2
1.5
1
0.5
0
2D
4D
6D
Control
nSD-HA<20
nSD-HA20/45
nSD-HA45/75
nSD-HA75/100
Samples

Fig. 9